Soft Matter

ARTICLE TYPE

Cite this: DOI: 10.1039/xxxxxxxxxx

Scale-dependent interactions enable emergent microrheological stress response of actin-vimentin composites

Julie Pinchiaroli*, Renita Saldanha†, Alison E Patteson†, Rae M. Robertson-Anderson‡ and Bekele J. Gurmessa*

* *Department of Physics and Astronomy, Bucknell University, Lewisburg, PA, 17837, USA.*
† *Department of Physics and BioInspired Institute, Syracuse University, Syracuse, NY 13210, USA.*
‡ *Department of Physics and Biophysics, University of San Diego, San Diego, CA 92110, USA.*

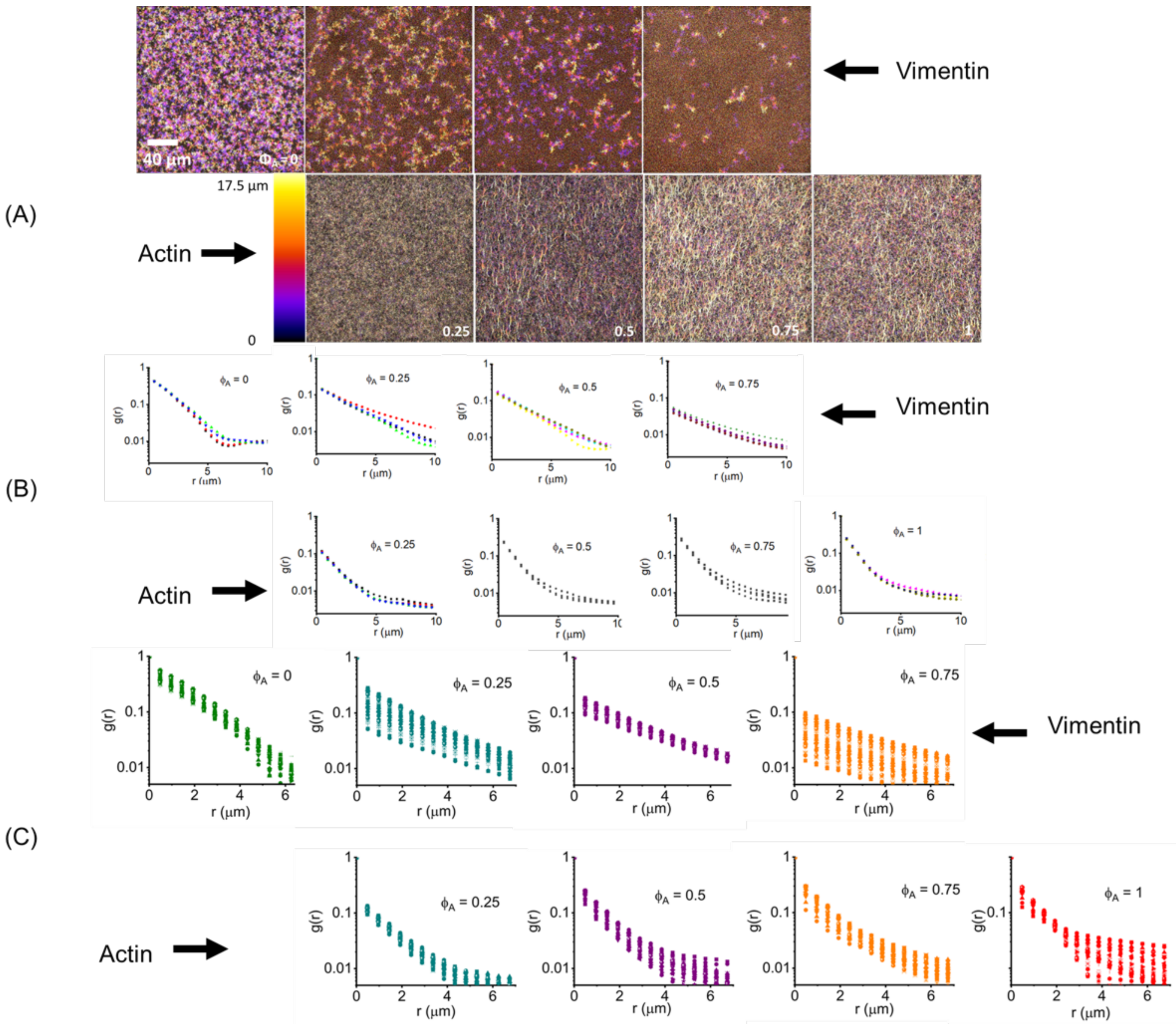

Fig. 1 S1: (A) Confocal images of two single channels (vimentin, top row and actin, bottom row) which correspond to each composite image shown in Fig 1 in the main text. The images shown here are temporally color-coded by z-height to illustrate the 3D structure. (B) SIA plots for vimentin (top row) and actin (bottom row) obtained from the greyscale of the single-channel images displayed in (A) after dividing them into quadrants for each channel. The g(r) for each quadrant was overlaid to show the variation in spatial heterogeneity. (C) SIA (g(r)) plots obtained from the full field of view of 3D confocal videos consisting of 35 frames of vimentin (top row) and actin (bottom row). The g(r) for each composition was displayed to demonstrate the variation between images in z-sectioning.

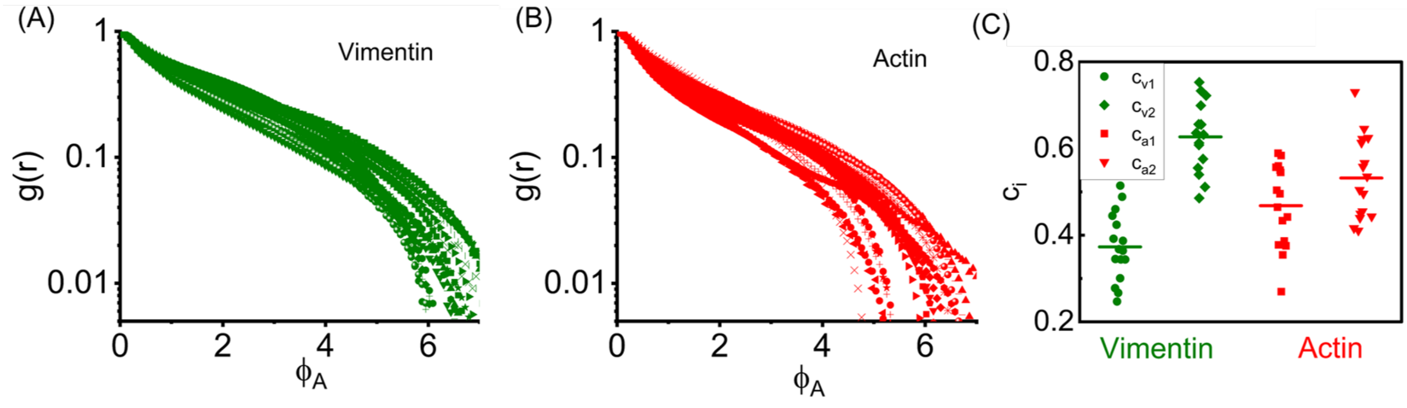

Fig. 2 S2: *In vivo* SIA data for individual trials of (A) vimentin, (B) actin, and (C) the relative weighting factor extracted by curve fitting the data in (A) and (B) to a double exponentially decaying function, as described in the main paper.

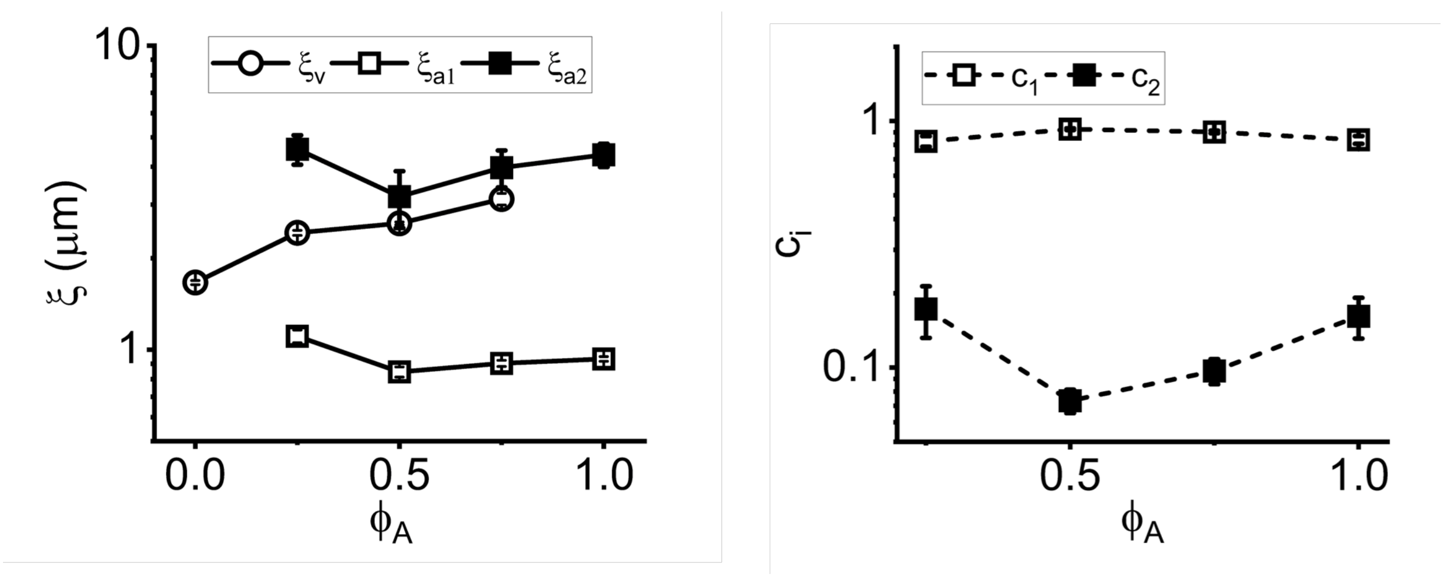

Fig. 3 S3: Correlation length (left) and the relative weighting factor (right) of *in vitro* samples whose SIA data is displayed in Fig S1C. They are extracted by curve fitting to a single exponentially decaying function for vimentin and a double exponentially decaying function for actin, as described in the main paper.

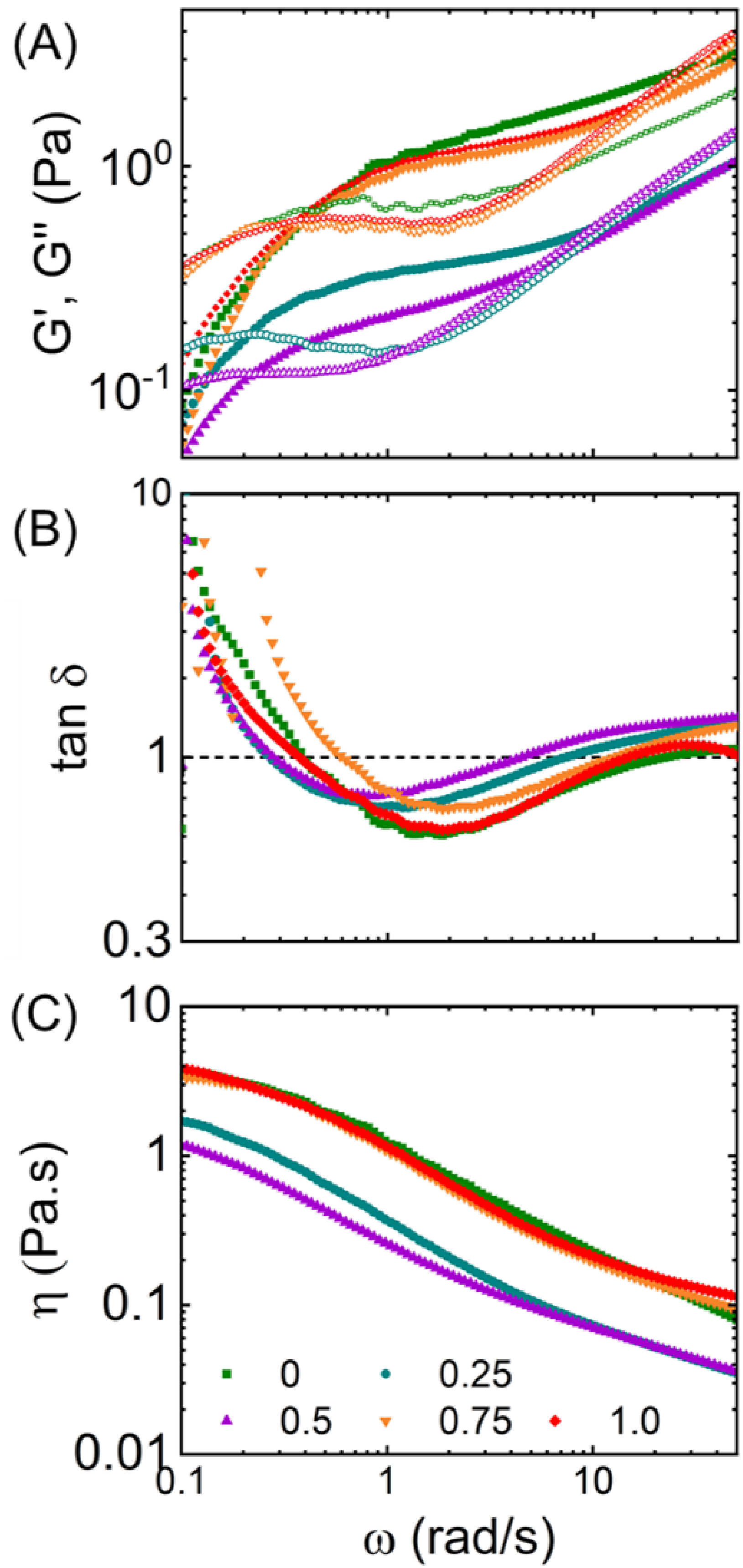

Fig. 4 S4. (A) Linear frequency-dependent elastic modulus G' (closed symbols) and viscous modulus G'' (open symbols) of the actin-vimentin composite networks, (B) Frequency-dependent loss tangent $tan\ \delta = G''(\omega)/G'(\omega)$ versus ω computed from data shown in (A) with a dashed black line representing $G' = G''$, indicating the extent to which each system exhibits elastic versus viscous dynamics of F-actin-vimentin composite, (C) Frequency-dependent shear viscosity $\eta(\omega)$. Each composition is the average of 20 different trials, as explained in the methods section of the main text.

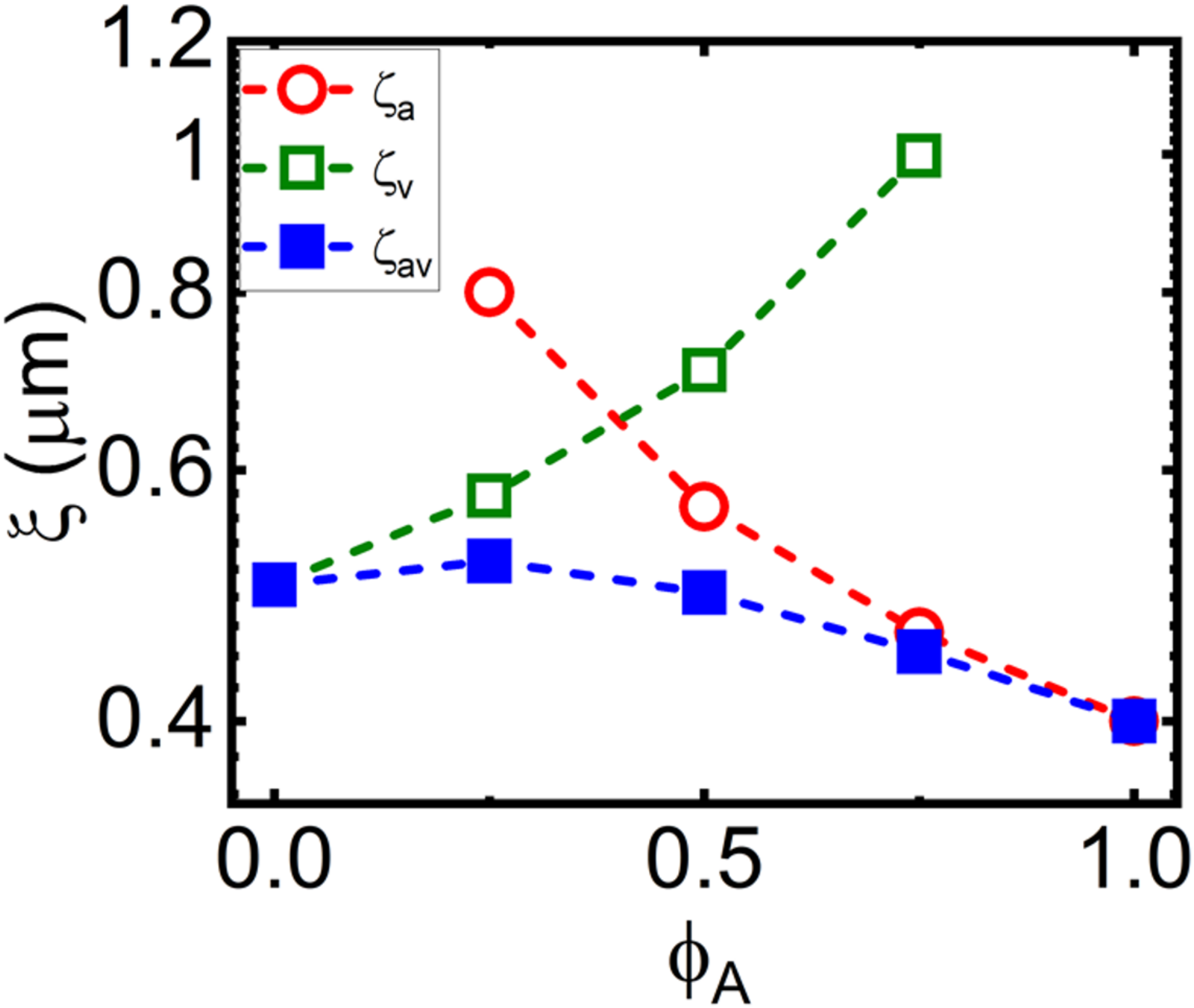

Fig. 5 S5: The computed mesh sizes of actin (ξ_A), vimentin (ξ_V), and the actin-vimentin composite (ξ_c) networks, which represent the average distance between adjacent entanglement points, were determined as described in the main text. The mesh size of actin, ξ_A, decreases as the concentration of actin (ϕ_A) increases, while the mesh size of vimentin, ξ_V, increases. However, the overall mesh size of the composite, ξ_c, remains approximately the same ($\xi_c = [\xi_A^{-3} + \xi_V^{-3}]^{-1/3} \approx 0.5\ \mu$m).

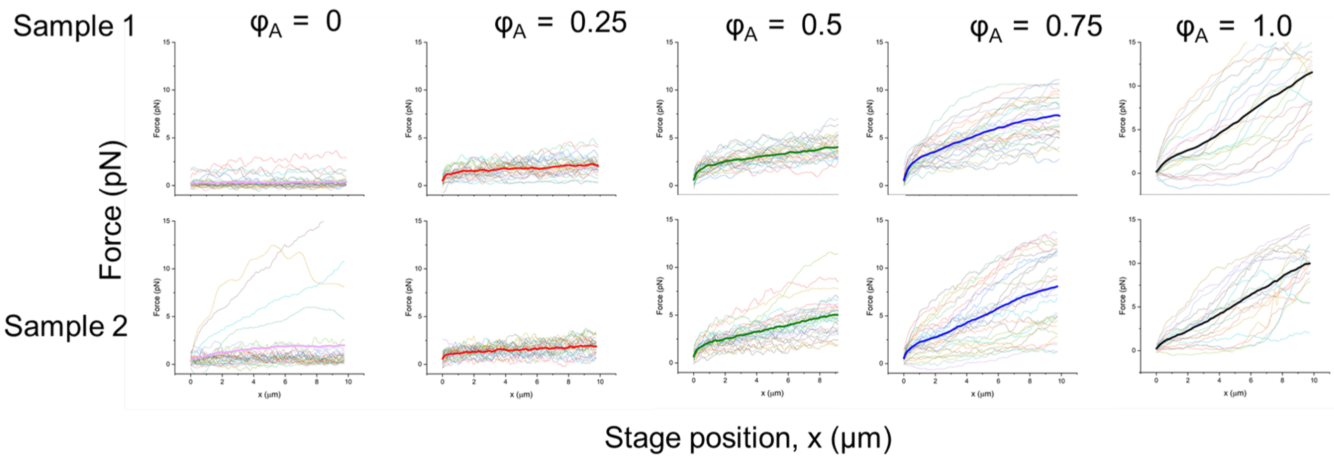

Fig. 6 S6. Individual force trials that are averaged over to compute the average force curves F(x) shown in Fig 4A. Each trial uses a different microsphere probe in a different region of the sample chamber. Each panel corresponds to a different combination of ϕ_A (columns) and the two replicates (rows) as indicated on the top and left of the panel grid.

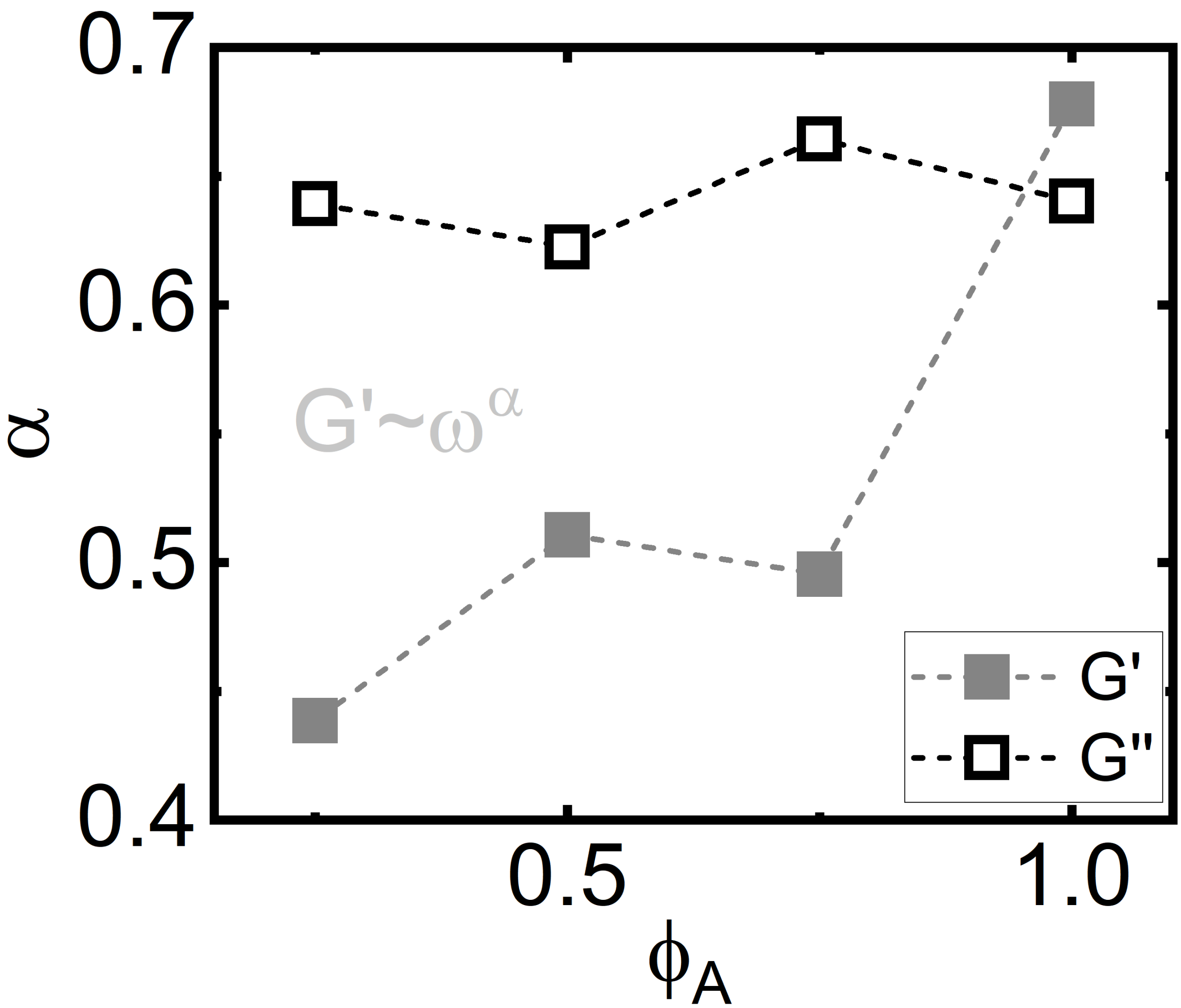

Fig. 7 S7: Scaling exponent obtained by fitting to power laws as $G' \sim \omega^{\alpha}$ and $G'' \sim \omega^{\beta}$ in the high-frequency regimes starting from where G'' exceeds G' as displayed in SI Fig S4(A).